Jestr

Journal of Engineering Science and Technology Review 16 (4) (2023) 77 - 84

Research Article

JOURNAL OF
Engineering Science and Technology Review

www.jestr.org

A Study of 1-Methylbenzotriazole (MEBTA) Using Quantum Mechanical Calculations and Vibrational, Electronic, and Nuclear Magnetic Resonance Spectroscopies

A. Dimitropoulos[1], Ch. Stamou[1], Sp. P. Perlepes[1], Z. G. Lada[1,2], I. D. Petsalakis[3] and S. Marinakis[1,4*]

[1]*Department of Chemistry, University of Patras, Patras GR-26504, Greece*
[2] *Laboratory of Applied Molecular Spectroscopy, Institute of Chemical Engineering Sciences Foundation for Research and Technology Hellas (FORTH/ICE-HT), Patras GR-26504, Greece*
[3]*Theoretical and Physical Chemistry Institute, National Hellenic Research Foundation, 48 Vassileos Constantinou Ave., Athens 116 35, Greece*
[4]*School of Health, Sport and Bioscience, University of East London, Stratford Campus, Water Lane, London E15 4LZ, UK*

Received 3 June 2023; Accepted 26 August 2023

Abstract

Infrared, Raman, UV-VIS, ^{1}H and ^{13}C NMR spectroscopic properties of 1-Methylbenzotriazole (MEBTA) are reported using experimental and computational methods. Density functional theory (DFT) using various functional and basis sets was employed to model the experimental data. The experimental vibrational and NMR data were in very good agreement with the DFT predictions. The 6-311+G(d,p) basis set was found to be adequate for this study in conjunction with the B3LYP, BP86, and CAM-B3LYP functionals. The effects of the solvation of MEBTA in various solvents were also investigated using UV-VIS experiments and calculations. The time-dependent DFT results qualitatively agree with the UV-VIS experimental data and are consistent with $\pi^* \leftarrow \pi$ transitions.

Keywords: 1-Methylbenzotriazole (MEBTA), Infrared, Raman, UV-VIS, NMR, DFT calculations

1. Introduction

Benzotriazole (BTAH, Fig. 1) and its various derivatives are ubiquitous compounds in almost all branches of Chemistry. They consist of a six-membered benzene ring fused at the 4,5-positions of a five-membered 1,2,3-triazole ring. The benzenoid form (left in Fig. 1) is more stable than the quinonoid form (right in Fig. 1) in the parent molecule (by around 9.5 kcal/mol); a consequence of this is that most derivatives of BTAH appear as the N(1)-isomer [1]. However, the proportion of the N(2)-isomer increases as the steric bulk of the N-substituent increases. The molecule can act as a weak acid ($pK_a = 8.2$) for proton loss or a very weak base for proton addition. It is insoluble in water, but due to its acid/base properties, is soluble in aqueous Na_2CO_3 and HCl.

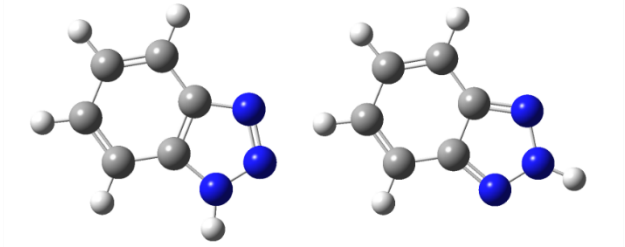

Fig. 1. The two tautomeric forms of BTAH. Note that the equilibrium is significantly shifted towards the left form. (Color online; H atoms = white spheres, C = grey spheres, and N = blue spheres).

BTAH is extremely popular in Organic Chemistry. It is soluble in most organic solvents, easy to synthesize, inexpensive, and chemically and thermally stable. Most importantly, the molecule is both electron donating resulting in acyl, aroyl, phosphonyl and sulfonyl derivatives of synthetic importance, and electron attracting thus stabilizing carbanions. The benzotriazolate anion (BTA^-) is a good leaving group and it can be used in place of halogen substituents in a plethora of reactions; the benzotriazolyl derivatives are much more stable than their chloro and bromo analogues [1,2]. 1-hydroxybenzotriazole (-N(OH) instead of -N(H) in Fig. 1) is an excellent synthetic auxiliary in the preparation of peptides [2]. In the field of Medicinal Chemistry, benzotriazole derivatives exhibit a variety of antimicrobial, antiparasitic, and even antitumor, choleretic, and cholesterol-lowering properties [3, 4].

In the field of Materials Chemistry, benzotriazoles find widespread applications, including: (a) Orthohydroxyphenyl benzotriazoles are commonly used as UV absorbers (stabilizers) in plastic materials, biosolids and personal care products [5]. (b) Benzotriazole-decorated graphene oxide is an efficient material for the removal of hexavalent uranium from nuclear wastewater [6]. (c) BTAH and its benzene ring amino, azido and nitrosubstituted derivatives, as well nitrogen-rich azole substituted derivatives have been tested for energetic material applications [7]. (d) Polar benzotriazoles, including BTAH, are used as corrosion inhibitors for metals (especially Cu), in antifreeze liquids, aircraft de-icing fluids, household detergents for dishwashing

*E-mail address: s.marinakis@upatras.gr
ISSN: 1791-2377
doi:10.25103/jestr.164.10

machines and in several industrial systems such as cooling, braking, and cutting [8, 9].

Benzotriazole- and benzotriazolate-based ligands are also central 'players' in the field of Inorganic Chemistry [10]. They have been used in the synthesis of coordination clusters [11, 12, 13, 14] with aesthetically beautiful structures (e.g. cyclic coordination cages and Kuratowski-type complexes) and exciting properties (e.g. magnetic and photophysical). The positions of the N atoms in the azole ring impose a bridging behavior and the deprotonated benzotriazoles have been identified as suitable linkers towards the formation of coordination polymers [15, 16], some of them having interesting optical and magnetic properties.

The physical chemistry (including theoretical studies) of benzotriazoles and its N-substituted derivatives has been less studied. An early theoretical work of benzotriazoles and its N-substituted derivatives [17] provided an explanation for the extraordinary difference in stability between 1,2,3-triazole and benzotriazole; in the latter the 1H tautomer represents more than 99.99% of the equilibrium mixture in the gas phase. The UV absorption spectra of BTAH and 1-methylbenzotriazole (MEBTA, -NCH_3 instead of -NH in Fig. 1 (left)) are very similar to one another [18, 19, 20]. The ^{1}H NMR spectrum of MEBTA in the aromatic region is quite different from that of the parent BTAH compound [19]. ^{1}H NMR [21] and detailed ^{13}C and ^{15}N NMR assignments have been reported [22, 23, 24]. The electronic structures and relative stabilities of BTAH and its N-substituted derivatives (including MEBTA) have been studied by UV Photoelectron Spectroscopy (UPS) and high-level ab initio methods [25]; the extent to which substituents influence the electronic structure of the benzotriazole skeleton depends on their mode of attachment to the skeleton. Concerning vibrational spectroscopy, FT-Raman and surface-enhanced Raman peaks of benzotriazoles have been tabulated and assigned [26, 27].

The present work aims to provide a joint experimental and theoretical study of MEBTA (Fig. 2), which is the archetype of N-substituted benzotriazoles. MEBTA is an almost white solid. For the human body, it is dangerous if ingested, causes irritation upon contact with the skin and more seriously with the eyes; moreover, it can be harmful to the respiratory system. The coordination chemistry of MEBTA has been intensely studied [28], mainly by Perlepes and coworkers [29, 30, 31, 32, 33]. A common feature in all studies is the monodentate ligation of MEBTA, the donor atom being the N atom of position 3 of the azole ring (N1 in the numbering scheme used in the present work, Fig. 2); this monodentate coordination has been related to the inability of MEBTA to act as corrosion inhibitor for copper, its alloys, and other metals. The general lack of spectroscopic (both experimental and theoretical) for MEBTA prompted us to undertake this study. All the experiments were carried out at room temperature and were accompanied with Density Functional Theory (DFT) calculations employing various functionals and basis sets, performed to provide the optimized geometry and the spectra.

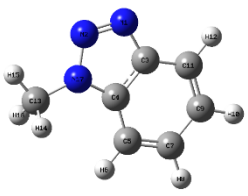

Fig. 2. The structural formula of 1-methylbenzotriazole (MEBTA). The atomic labelling scheme is as used in the calculations in this work.

2. Materials and Methods

2.1. Experimental Details

Solid MEBTA (Alfa Aesar, 98+%) was purchased and used as received for all the measurements. The solvents were not purified further. The Fourier-transform infrared (FT-IR) spectroscopy measurements were done in the 4000–400 cm-^{1} region using the Thermo Scientific (Nicolet iS20) spectrometer. A fast-recovery deuterated triglycine sulfate (DTGS) detector was used to record the infrared spectrum in transmittance form with a resolution of 4cm^{-1}. Because of the good signal-to-noise ratio, the number of scans (signal and background) was set to 12. For the Raman measurements, the T64000 Horiba Jobin Yvon micro-Raman setup was used. The excitation wavelength was the 514.5 nm emitted from a DPSS laser (Cobolt Fandango TMISO laser, Norfolk, UK). The laser power on the sample was 2 mW. Prior photo-bleaching of the sample was crucial in order to avoid the in-parallel phenomenon of fluorescence existing in the sample. The backscattered radiation was collected from a single configuration of the monochromator after passing through an appropriate edge filter (LP02-633RU-25, laser2000, UK, Ltd., Huntingdon, Cambridgeshire, UK). The calibration of the instrument was achieved via the standard Raman peak position of Si at 520.5cm^{-1}. The spectral resolution was 5cm^{-1}. NMR spectra in d_6-DMSO were recorded using a Bruker Avance DPX spectrometer (400.13 MHz for ^{1}H NMR and 100.62 MHz for ^{13}C NMR). UV spectra were recorded for MEBTA solutions with the following concentrations: 0.3 mM (in MeOH), 0.53 mM (in MeCN), 0.038 mM (in DMSO), and 0.11 mM (in DMF). The spectral region measured was 190-800 nm and the spectrometer used was Analytik Jena (Specord 50 Plus).

2.2. Computational Details

Theoretical DFT calculations are employed in order to calculate the optimised three-dimensional geometry and the spectroscopic properties of MEBTA. In order to calculate the geometry, we used as starting point the coordinates of the atoms of MEBTA as provided in the crystallographic file (ja9041093_si_002.cif) by Duan et al. [34], where BTA^- was a ligand in a Au(I) complex. The structural formula of MEBTA and the atomic labelling scheme is shown in Fig. 2. All calculations were carried out using the Gaussian 16W program, version 1.1 [35] and the visualizations were done using the GaussView, version 6.1 [36]. The calculations employed the B3LYP, BP86, CAM-B3LYP functionals in conjunction with the 6-31G(d,p), 6-311G(d,p), and 6-311+G(d,p) basis sets. Using the default settings in the Gaussian 16W program, the NMR calculations were performed using the Gauge-independent atomic orbital (GIAO) approximation [37, 38, 39]. The effects of the solvents were calculated using the default polarizable continuum model (PCM) [40] only for the NMR and UV-VIS spectra. Gas phase calculations, without taking into account any solvent effects, were employed for the geometry, and the IR / Raman predictions. Our calculations consider only MEBTA and not its dimer because of the small concentrations of MEBTA in the UV-VIS and NMR experiments in the liquid phase. In the case of IR / Raman experiments in the solid phase, the dimer may exist. However, the agreement between the monomer calculations and the experimental results indicated that the effects of the dimer on the vibrational spectra are small.

3. Results and Discussion

3.1. Geometry

The X, Y, Z coordinates of the optimised geometry are presented in Tables S1-S9 for the nine combinations of the three functionals, B3LYP, BP86, and CAM-B3LYP, with the three basis sets, 6-31G(d,p), 6-311G(d,p), and 6-311+G(d,p). The atomic labelling is as in Fig. 2. The values of the bond lengths are shown in Fig. 3 and of the angles in Fig. S1 in the supplementary material. The values of the dihedral angles are shown in Fig. S2. According to the convention in Gaussian 16W, the bond angles take values in the [0°, 180°], and the dihedral angles in the [-180°, 180°] ranges, respectively.

Comparing the predictions of the bond lengths from the various basis sets (Fig. 3), the smallest basis set produces the largest value. The other two, larger basis sets converge in their predictions. Comparing the predictions between the various functionals, the CAM-B3LYP method gives the shortest bond lengths, and the BP86 method gives the largest. The values of the C-H bond lengths are as expected (109 pm) for C (sp^2). The values for the C-C bonds are as expected (140 pm) for aromatic carbon atoms in a benzene ring [41]. The three C-H bonds of the methyl group are longer than the rest C-H because C has an sp^3 hybridization. From the two N-N bonds in the triazole ring, N1-N2 is shorter than N2-N17. Regarding the C-N bonds, we note that C3-N1 is very short.

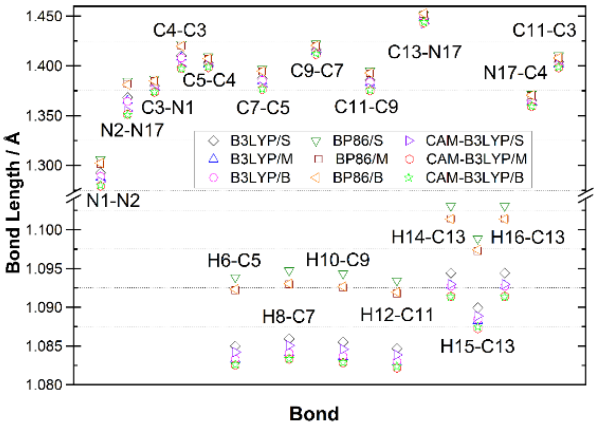

Fig. 3. Calculated bond lengths (in Å) of MEBTA. The DFT functionals are shown in the inset. The S, M, και B symbols represent the 6-31G(d,p), 6-311G(d,p), and 6-311+G(d,p) basis sets, respectively. The Y-axis is not drawn continuously, and the scale is different before and after the break.

Regarding the angles in the benzene ring (Fig. S1), the three functionals give similar values. This agreement between the three functionals gets worse when the angles in the triazole ring are compared. The values of the dihedral angles (Fig. S2) indicate that the triazole ring adopts a planar geometry too, and the two rings are in the same plane.

3.2. Vibrations

The experimental infrared (IR) spectrum of the solid MEBTA is shown in Fig. 4, and the experimental Raman spectrum is presented in Fig. 5. A comparison between the experimental Raman peaks and the theoretical predictions from all functionals using the largest basis set, 6-311+G(d,p), is shown in Fig. 6. The B3LYP functional reproduces the Raman experimental data better than the rest functionals. The vibrational assignment of eighteen FT-IR and fifteen Raman peaks along with a comparison with the B3LYP predictions is shown in Table 1. The peak assignments were made using Socrates [42] and the work by Thomas et al. [26] on the related BTAH molecule.

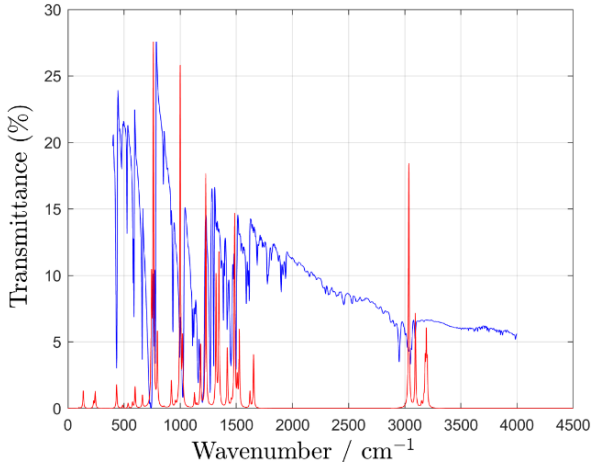

Fig. 4. Comparison between experimental (blue online) IR spectrum (transmittance %) of solid MEBTA and theoretical absorption (red online). The theoretical data have been scaled by 0.1255 to aid comparison.

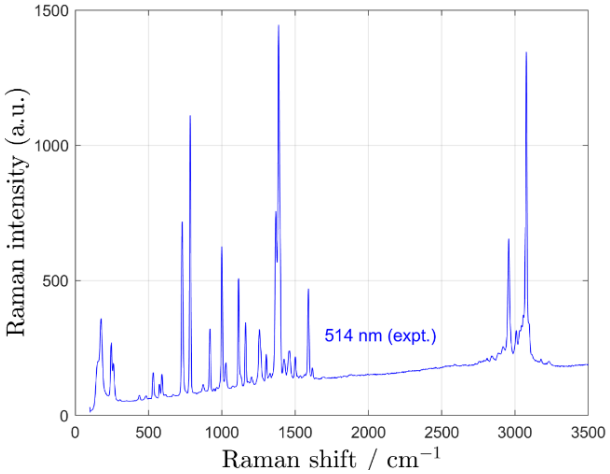

Fig. 5. Raman spectrum (experimental) of solid MEBTA.

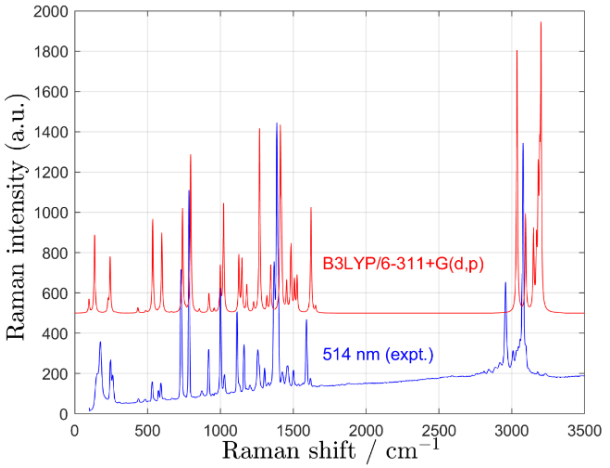

Fig. 6. Comparison between the experimental Raman spectra of solid MEBTA with theoretical calculations using B3LYP/6-311+G(d,p) level of theory.

In general, the experimental data are in good agreement with the literature regarding the positions of the vibrational peaks. The highest discrepancies were observed only for the highest frequency values. In that frequency region, it is well known [43] that quantum mechanical calculations usually predict vibrational frequencies with values larger than the experimental ones due to the negligence of anharmonicity effects, and the approximations made regarding the electron correlation. No scaling was applied in our computational results in order to allow a direct comparison with experiments; the calculated vibrational wavenumbers are typically larger than those observed experimentally. Regarding the experimental values, the aromatic =C-H (3000 - 3100 cm^{-1}) and the aliphatic (2900 - 3000 cm^{-1}) -C-H stretching vibrations were measured. In the region 1500 - 1650 cm^{-1}, the C=C and C=N bond stretching were observed. The saturated aliphatic C-H deformations and the C-N stretching appear in the region 1300 - 1450 cm^{-1}. The aromatic C-H in-plane and out-of-plane deformations are shown in the 1000 - 1250 and 700 - 1000 cm^{-1} intervals, respectively. Thomas et al. [26] suggested that the weak peak around 1160 cm^{-1} corresponds (except to =C-H in-plane deformation as shown in Table 1) to NNN symmetric stretch (triazole ring breathing). The C=N and N=N stretching vibrations appear at around 650 cm^{-1}. In the region below 600 cm^{-1}, we see deformations and librations.

Table 1. Vibrational assignment for the experimentally observed FT-IR and Raman wavenumbers (cm^{-1}) and comparison with B3LYP/6-311+G(d,p) calculations. Relative intensities are denoted by vs (very strong), s (strong), m (medium), w (weak), vw (very weak), and vr (variable). The width of the peak is denoted by b (broad), and sh (sharp).

Experimental IR	**Experimental Raman**	**Assignment**	**B3LYP/6-311+G(d,p) IR**	**B3LYP/6-311+G(d,p) Raman**
3050w-b	3077vs-b	=C-H stretching [ring]	3191m	3200vs, 3181vs
2950w-sh	2957s-sh	C-H asymmetric stretching [CH_3]	3094m	3094s 3036vs (symmetric)
1614m-b	1591m-sh	-C=C- stretching [ring] C=N stretching	1653w	1622m
1589m-b		-C=C- stretching [ring] C=N stretching	1622vw	
1496s-sh		-C=C- stretching [ring] C=N stretching N=N stretching	1526m + C-H stretching [CH_3]	
1452s-b	1462w	C-H asymmetric deformation [CH_3] -C=C- stretching [ring]	1483s + C-H in-plane deformation [ring]	1486w (asymmetric) 1455w + C-H in-plane deformation [ring]
	1387vs-b	C-H sym deformation [CH_3]		1419m, 1483w -C=C- stretching + C-H in-plane deformation [ring]
	1368s-b	C-N stretching C-H sym deformation [CH_3]	1345s + C-H in-plane deformation [CH_3, ring]	
1299s-sh		C-N stretching	-	
1267vs-sh	1255w-sh	=C-H in-plane deformation [ring]	1228vs	1269m
1197vs-b		=C-H in-plane deformation [ring]	1181vw	
1160vs-b	1161w-sh	=C-H in-plane deformation [ring]	-	1127vw
	1114m-sh	=C-H in-plane deformation [ring]		-
1024vs-b		=C-H in-plane deformation [ring]	1000s-b	
995s-b	1000s-sh	=C-H in-plane deformation [ring]	1000s-b	1000w
935s-sh	919w-sh	=C-H out-of-plane deformation [ring]	956vw	956vw
779vs-b	783vs-sh	=C-H out-of-plane deformation [phenyl ring]	855vw	855vw
740vs-b		=C-H out-of-plane deformation [ring]	761vs	
	730s-sh	=C-H out-of-plane deformation [ring]		745vw + out-of-plane deformation of benzene ring
661vs-sh		C=N and N=N stretching		
588s-sh		aromatic ring in-plane deformation	598vw	598vw
433vs-sh		aromatic ring out-of-plane deformation	434vw	434vw
	245w-b	in-plane libration [CH_3]		243vw in-plane deformation [CH_3 and benzene ring]
	176w-b	out-of-plane libration [CH_3]		136vw out-of-plane deformation [CH_3 and benzene ring]

3.3. Nuclear Magnetic Resonance (NMR) results

The results using 6-31G(d,p) were far away from the results from the other two, larger basis sets. The values from the 6-311G(d,p), while converging well with those of the 6-311+G(d,p), did not correlate well with the literature. The obtained calculated ^{1}H NMR and ^{13}C NMR chemical shifts using the 6-311+G(d,p) basis set are in good agreement with experimental shifts from this work and previous measurements [21, 22, 23] as shown in Tables 2 and 3, respectively. The chemical shifts δ (ppm) were calculated using tetramethylsilane (TMS) as the reference compound. The resonance frequency of the reference compound was calculated using the default setting in Gaussian 16W, i.e. the B3LYP/6-311+G(2d,p) GIAO method. This means that the reference compound NMR frequencies were calculated using a different basis set from the calculations (it includes different polarization functions, in particular, it adds an extra set of d functions to the heavy atoms). In our case, however, the difference between the two sets is insignificant. The use of the same method for the reference compounds of all calculations makes it easier to compare the final results with each other.

Table 2. Comparison between the calculated chemical shifts, δ (in ppm), of the ^{1}H NMR spectrum of MEBTA using B3LYP, BP86, and CAM-B3LYP functionals in combination with the 6-311+G(d,p) basis set with experimental values from this work. For the calculated values in the last line, the δ value is the average of the H14, H15, and H16 values.

H-atom	B3LYP	BP86	CAM-B3LYP	Experimental value [21]	Experimental value [This work]
H12	8.21	8.48	8.33	7.93	8.00, d
H8	7.57	7.87	7.66	7.25	7.55, t
H6	7.46	7.82	7.53	7.32	7.81, d
H10	7.44	7.78	7.49	7.37	7.40, t
H15	4.78	5.15	4.80		-
H16	3.83	4.22	3.81		-
H14	3.83	4.22	3.81		-
Averaged H(CH_3)	4.15	4.53	4.14		4.28, s

Table 3. Comparison between the calculated chemical shifts, δ (in ppm), of the ^{13}C NMR spectrum of MEBTA using B3LYP, BP86, and CAM-B3LYP functionals, in combination with the 6-311+G(d,p) basis set, with results from a previous experimental study [22] and this work.

C-atom	B3LYP	BP86	CAM-B3LYP	Experimental value [22]	Experimental value [This work]
C3	153.06	151.51	150.20	145.5	145.3
C4	138.45	135.73	136.45	133.1	133.5
C7	131.01	128.69	130.09	126.8	127.2
C9	126.83	125.40	125.08	123.4	124.0
C11	126.08	123.93	125.59	119.3	119.1
C5	110.59	109.40	109.13	108.8	110.7
C13	33.67	35.10	29.47	33.7	34.2

The ^{1}H NMR experimental resolution from this work allowed the observation (in order of decreasing δ): a doublet peak for H12 (due to coupling with H10), a triplet peak for H8 (due to coupling with H6, H10), a double peak for H6 (due to coupling with H8), a triplet peak for H10 (due to coupling with H8, H10), and only one (averaged) peak for the three hydrogens bonded to the methyl carbon. The order of the average ^{1}H NMR chemical shift (ppm) values was: B3LYP (6.16) < CAM-B3LYP (6.20) < experimental (6.23) < BP86 (6.51).

The ^{13}C NMR results showed that the highest δ values are for the two C atoms (C3 and C4) which connect the two rings. The values for the phenyl carbons (C5, C7, C9 and C11) are between 131 and 109 ppm, with the carbon C5, which is closest to the methyl group, taking the lowest value. As expected, the chemical shift value of the methyl carbon was the lowest. The order of the average ^{13}C chemical shift (ppm) values was: experimental (113.4) < CAM-B3LYP (115.1) < BP86 (115.7) < B3LYP (117.1).

3.4. Electronic Spectroscopy Results

The calculations provided the oscillator strength, f, and the molar absorption coefficient, ε (L mol^{-1} cm^{-1}) versus wavelength. The theoretical calculations presented are in the region ~190 - 350 nm (the calculations were performed in the region ~100 - 800 nm, but there was no absorption at larger wavelengths). Calculations were performed for the system in the gas phase and in four solvents. The default values of the relative permittivity (dielectric constant) used in Gaussian 16W [35] and the electric dipole moment values (in D) [41] are: ethanol (EtOH, 24.852, 1.69), acetonitrile (MeCN, 35.688, 3.92), dimethyl sulfoxide (DMSO, 46.826, 3.96), and acetone (Me_2CO, 20.493, 2.88). The time-dependent DFT (TD-DFT) method was applied to calculate the electronic absorption spectrum of MEBTA by taking into account the 10 singlet-to-singlet spin-allowed lowest energy states. UV-VIS spectra were recorded for four solvents: methanol (MeOH, 32.613, 1.70), MeCN, DMSO, and N,N-dimethylformamide (N,N-DMF, 37.219, 3.82). Experimental spectra are shown in Fig. 7 and data are listed in Table 4.

Rotationally resolved UV spectroscopy of the 2H-tautomer of benzotriazole was reported by Berden et al. [44]. Regarding the UV-visible spectra of MEBTA, previous work [18] has shown that it has two maxima in methanol solvent at 254 nm (log ε = 3.82) and 284 nm (log ε = 3.66). Two decades later, Roberts measured the following values for λ_{max} (nm) and 10^{-3} ε: 256.4 (6.78), 262.0 (6.82), and 279.2 (5.10) [19]. In a review of work prior to 1971 [45 and references therein], Armarego reported the values 255 nm (log ε = 3.81), and 283 nm (log ε = 3.68). Catalán et al. measured the UV-VIS in the gas phase and found that λ_{max} = 247 nm, a nearby shoulder at 254 nm, and another peak at 282 nm [20]. Tomás et al. measured again the UV-VIS spectrum at 90°C and the fluorescence spectrum at 90°C [46]. Novak et al. measured UV photoelectron spectroscopy (UPS) and performed high-level ab initio calculations to examine the relative stability of the N-substituted benzotriazoles [25].

The calculated maximum absorbance wavelength, λ, and f using the largest basis set, 6-311+G(d,p) for the functionals B3LYP, BP86, and CAM-B3LYP are shown in the Supplementary material in Tables S10, S11, and S12, respectively. The shapes of the HOMO-1 (orbital with cardinal number 34a), HOMO (35a), LUMO (36a), and LUMO+1 (37a) orbitals from the CAM-B3LYP/6-311+G(d,p) calculations in the gas phase are shown in Fig. 8. The electron transition between the HOMO and LUMO orbitals corresponds to -0.2892 eV. The calculated UV-visible band has a maximum at 177.2 nm, which consists of (the coefficients are in the parentheses): 32a→36a (0.34688), 34a→36a (-0.27210), 34a→39a (-0.30908), 34a→44a (0.19908), and 35a→39a (-0.34344). As shown in the orbital shapes in Fig. 8 and in Fig. S3 in the Supplementary material, the peak corresponds to π←π* transitions as suggested in previous studies for the 2H-tautomer of benzotriazole [44] and for the 1H- and 2H-benzotriazole [47].

Table 4. Experimental UV spectra of MEBTA in MeOH, MeCN, DMSO, και DMF. λ (nm) is the wavelength of a given point in the spectrum, ε (L mol^{-1} cm^{-1}) is the corresponding molar extinction coefficient value.

MeOH	ε	MeCN	ε	DMSO	ε	DMF	ε
205	7742.3	191	4934.5	254	18194.7	260	10190.0
210	8975.3	197	7017.7	256	27450.0	262	10778.2
255	4710.7	203	6996.8	259	43960.5	265	14016.4
263	4928.0	205	6894.2	261	45028.9	267	16347.3
280	3669.7	208	6675.5	263	45531.6	269	17614.5
		213	6498.7	265	46344.7	283	17524.5
		256	5401.9	284	35039.5		
		262	5371.3				
		283	4111.7				

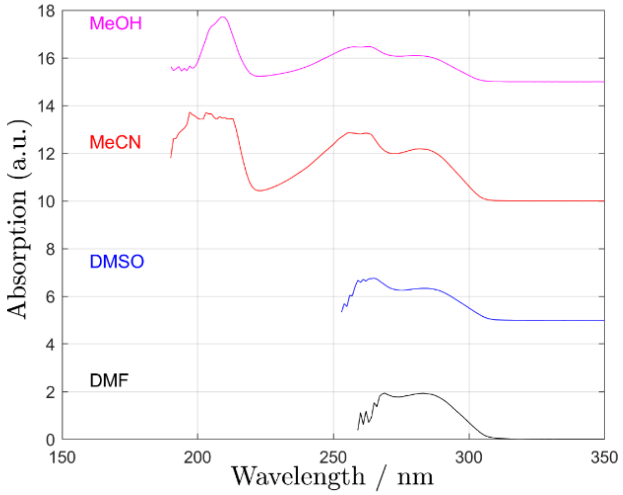

Fig. 7. Experimental UV-visible absorption spectra of MEBTA in (from top to bottom): MeOH, MeCN, DMSO, and DMF.

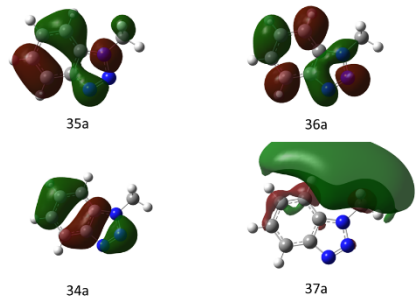

Fig. 8. The frontier molecular orbitals of MEBTA from CAM-B3LYP/6-311+G(d,p) calculations in the gas phase: HOMO-1 (34a) -0.26346 eV, HOMO (35a) -0.24853 eV, LUMO (36a) -0.05712 eV, LUMO+1 (37a) -0.00863 eV.

4. Conclusions

To summarize, the MEBTA molecule was studied using DFT calculations and IR / Raman, UV-VIS, and NMR experiments. The optimized three-dimensional structure was calculated by DFT. The agreement between experimental and theoretical results for the vibrations was good with theory overpredicting wavenumbers values only in the region around and over 3000 cm^{-1}. Regarding the comparison among the different DFT functionals, we note that, on average, the best agreement with the experiments was with B3LYP for vibrations and with CAM-B3LYP for NMR. The UV-VIS experimental results qualitatively agree with time-dependent DFT calculations, which suggest π*←π transitions.

Acknowledgments
We thank Maria Iliopoulou and Ioanna Valavani (U. of Patras) for helping with some experiments.

Appendix A. Supplementary data
Supplementary data associated with this article can be found, in the online version, at [Tables 1S-9S: Optimized geometries; Tables 10S-12S: Calculated maximum absorbance wavelength; Fig. 1S: Bond angles; Fig. 2S: Dihedral angles; Fig. 3S: The first 46 lowest molecular orbitals.]

References

[1] C. D. Hall, S. S. Panda, "The benzotriazole story", *Adv. Heterocycl. Chem.*, vol. 119, pp. 1-23, May, 2016, doi: 10.1016/bs.aihch.2016.01.001
[2] A. R. Katritzky, S. Rachwal, G. J. Hitchings, "Benzotriazole: a novel synthetic auxiliary", *Tetrahedron*, vol. 47, no 16, pp. 2683-2732, 1991, doi: 10.1016/S0040-4020(01)87080-0
[3] P. K. Patel, P. D. Patel, S. Patel, "Synthesis, characterization, chelating properties and biological activities of benzotriazole-salicylic acid combined molecules", *Int. J. Pharm. Chem. Sci.*, vol. 1, no. 4, Oct., 2012, pp. 1799-1804
[4] I. Briguglio, S. Piras, P. Corona, E. Gavini, M. Nieddu, G. Boatto, et al., "Benzotriazole: An overview on its versatile biological behavior", *Eur. J. Med. Chem.*, vol. 97, Jun., 2015, pp. 612-648, doi: 10.1016/j.ejmech.2014.09.089
[5] M. J. Paterson, M. A. Robb, L. Blancafort, A. D. DeBellis, "Theoretical study of benzotriazole UV photostability: Ultrafast deactivation through coupled proton and electron transfer triggered by a charge-transfer state", *J. Am. Chem. Soc.*, vol. 126, no. 9, Mar., 2004, pp. 2912-2922, doi: 10.1021/ja0386593
[6] J. Ding, Z. Yan, L. Feng, F. Zhai, X. Chen, Y. Xu, et al, "Benzotriazole decorated graphene oxide for efficient removal of U(VI)", *Environ. Pollut.*, vol. 253, Oct., 2019, pp. 221-230, doi: /10.1016/j.envpol.2019.06.109
[7] D. Srinivas, V. D. Ghule, S. P. Tewari, K. Muralidharan, "Synthesis of amino, azido, nitro and nitrogen-rich azole-substituted derivatives of 1*H*-benzotriazole for high-energy materials applications", *Chem. Eur. J.*, vol. 18, no. 47, Nov., 2012, pp. 15031-15037, doi: 10.1002/chem.201202481
[8] Z. Chen, L. Huang, G. Zhang, Y. Qiu, X. Guo, "Benzotriazole as a volatile corrosion inhibitor during the early stage of copper corrosion under adsorbed thin electrolyte layers", *Corros. Sci.*, 65, Dec., 2012, pp. 214-222, doi: 10.1016/j.corsci.2012.08.019
[9] A. Kokalj, "Ab initio modeling of the bonding of benzotriazole corrosion inhibitor to reduced and oxidized copper surfaces",

Faraday Discuss., vol. 180, Feb., 2015, pp. 415-438, doi: 10.1039/C4FD00257A

[10] E. Loukopoulos, G. Kostakis, "Recent advances in the coordination chemistry of benzotriazole-based ligands", *Coord. Chem. Rev.*, 395, Sep., 2019, pp. 193-229, doi: /10.1016/j.ccr.2019.06.003

[11] E. Diamantopoulou, C. P. Raptopoulou, A. Terzis, V. Tangoulis, S. P. Perlepes, "Heptanuclearity in nickel(II) chemistry: preparation, characterization, crystal structure and magnetic properties of $[Ni_7(OH)_2(acac)_8(btaO)_4(H_2O)_2]$", *Polyhedron*, vol. 21, no. 21, Sep., 2002, pp. 2117-2126, doi: 10.1016/S0277-5387(02)01158-0

[12] S. Biswas, M. Tonigold, H. Kelm, H. – J. Krüger, D. Volkmer, "Thermal spin-crossover in the $[M_3Zn_6Cl_6L_{12}]$ (M = Zn, Fe^{II}; L = 5,6-dimethoxy-1,2,3-benzotriazolate) system: structural, electrochemical, Mössbauer, and UV-Vis spectroscopic studies", *Dalton Trans.*, vol. 39, no. 41, Nov., 2010, pp. 9851-9859, doi: 10.1039/C0DT00556H

[13] T. W. Werner, S. Reschke, H. Bunzen, H. – A. Krug von Nidda, J. Deisenhofer, A. Loidl, et al., "$[Co_5Tp^*_4(Me_2bta)_6]$: A highly symmetrical pentanuclear Kuratowski complex featuring tris(pyrazolyl)borate and benzotriazole ligands", *Inorg. Chem.*, vol. 55, no. 3, Feb., 2016, pp. 1053-1060, doi: 10.1021/acs.inorgchem.5b01982

[14] G. J. Zhou, W. P. Chen, Y. Yu, L. Qin, T. Han, Y. Z. Zheng, "Filling the missing links of M_{3n} prototype 3d-4f and 4f cyclic coordination cages: syntheses, structures, and magnetic properties of the $Ni_{10}Ln_5$ and the Er_{3n} wheels", *Inorg. Chem.*, vol. 56, no. 21, Nov., 2017, pp. 12821-12829, doi: DOI: 10.1021/acs.inorgchem.7b01569

[15] K. Müller-Buschbaum, Y. Mokaddem, "MOFs by transformation of 1D-coordination Polymers: from $^1_\infty[Ln(Btz)_3BtzH]$ to the homoleptic rare earth 3D-benzotriazolate frameworks $^1_\infty[Ln(Btz)_3]$, Ln = La, Ce", *Z. Anorg. Allg. Chem.*, vol. 634, no. 12-13, Oct., 2008, pp. 2360–2366, doi: 10.1002/zaac.200800287

[16] Q. Y. Zhang, X. An, L. Xu, J. H. Yan, S. Zhang, W. Xie, Z. M. Su, "Syntheses, structure and properties of an especially stable Cd metal-organic framework driven by benzotriazole-5-carboxylic acid", *Inorg. Chem. Commun.*, vol. 112, Feb., 2020, Art. No. 107726, doi: /10.1016/j.inoche.2019.107726

[17] F. Tomás, J. L. M. Abboud, J. Laynez, R. Notario, L. Santos, S. O. Nilsson, et al., "Tautomerism and aromaticity in 1,2,3-triazoles: the case of benzotriazole", *J. Am. Chem. Soc.*, vol. 111, no. 19, Sep., 1989, pp. 7348-7353, doi: 10.1021/ja00201a011

[18] H. Specker, H. Gawrosch, "Über die ultraviolettabsorption der benztriazole, der pyridone und ihrer salze", *Chem. Ber.*, vol. 75, no. 11, Nov., 1942, pp. 1338-1348, doi: 10.1002/cber.19420751115

[19] N. K. Roberts, "Nuclear magnetic resonance and ultraviolet spectra of benzotriazole and its 1- and 2-methyl derivatives", *J. Chem. Soc.*, 1963, pp. 5556-5558, doi: 10.1039/jr9630005544

[20] J. Catalán, P. Pérez, J. Elguero, "Structure of benzotriazole in the gas phase: a UV experimental study", *J. Org. Chem.*, vol. 58, no. 19, Sep., 1993, pp. 5276-5277, doi: 10.1021/jo00071a046

[21] R. E. Rondeau, H. M. Rosenberg, D. J. Dunbar, "Nuclear magnetic resonance analysis of 1- and 2-methylbenzotriazole", *J. Mol. Spectrosc.*, vol. 29, no. 1-3, 1969, pp. 305-311, doi: https://doi.org/10.1016/0022-2852(69)90110-6

[22] M. Begtrup, R. M. Claramunt, J. Elguero. "Azolides. Part 12. Carbon-13 nuclear magnetic resonance study of N-methyl and N-acetyl derivatives of azoles and benzazoles", *J. Chem. Soc., Perkin Trans. 2*, 1978, pp. 99-104, doi: 10.1039/P29780000099

[23] M. Begtrup, J. Elguero, R. Faure, P. Camps, C. Estopá, D. Ilavský, et al., "Effect of N-substituents on the ^{13}C NMR parameters of azoles", *Magn. Reson. Chem.*, vol. 26, no. 2, Feb., 1988, pp. 134-151, doi: 10.1002/mrc.1260260210

[24] R. M. Claramunt, D. Sanz, G. Boyer, J. Catalãn, J. L. G. de Paz, J. Elguero, "Experimental (^{13}C and ^{15}N NMR spectroscopy) and theoretical (6-31G) study of the protonation of N-methylazoles and N-methylbenzazoles", *Magn. Reson. Chem.*, vol. 31, no. 9, Sep., 1993, pp. 791-800, doi: 10.1002/mrc.1260310902

[25] I. Novak, T. Abu-Izneid, B. Kovač, L.Klasinc, "Electronic structure and stability of benzotriazoles", *J. Phys. Chem. A*, vol. 113, no. 35, Sep., 2009, pp. 9751-9756, doi: 10.1021/jp905640b

[26] S. Thomas, S. Venkateswaran, S. Kapoor, R. D' Cunha, T. Mukherjee, "Surface enhanced Raman scattering of benzotriazole: a molecular orientational study", *Spectrochim. Acta A*, vol. 60, no. 1-2, Jan., 2004, pp. 25-29, doi: https://doi.org/10.1016/S1386-1425(03)00213-0

[27] D. Sockalingum, M. Fleischmann, M. M. Musiani, "Near-infrared Fourier transform surface-enhanced Raman scattering of azole copper corrosion inhibitors in aqueous chloride media", *Spectrochim. Acta A*, vol. 47, no. 9-10, 1991, pp. 1475-1485, doi: 10.1016/0584-8539(91)80239-F

[28] L. F. Jones, L. O' Dea, D. A. Offermann, P. Jensen, B. Moubaraki, K. S. Murray, "Benzotriazole based 1-D, 2-D and 3-D metal dicyanamide and tricyanomethanide coordination networks", *Polyhedron*, vol. 25, no. 2, Jan., 2006, pp. 360-372, doi: 10.1016/j.poly.2005.08.005

[29] E. Diamantopoulou, T. F. Zafiropoulos, S. P. Perlepes, C. P. Raptopoulou, A. Terzis, "Synthetic and structural chemistry of nickel(II)/1-methylbenzotriazole complexes", *Polyhedron*, vol. 13, no. 10, May, 1994, pp. 1593-1608, doi: 10.1016/S0277-5387(00)83455-5

[30] K. Skorda, E. G. Bakalbassis, J. Mrozinski, S. P. Perlepes, C. P. Raptopoulou and A. Terzis, "Copper(II) chloride–1-methylbenzotriazole chemistry: variation of product as a function of metal-to-ligand reaction ratio; synthesis, structure and properties of a dinuclear complex and a novel chain polymer with two alternating chromophores", *J. Chem. Soc., Dalton Trans.*, no. 13, pp. 2317-2319, Jul., 1995, doi: 10.1039/DT9950002317

[31] K. Skorda, T. C. Stamatatos, A. P. Vafiadis, A. T. Lithoxoidou, A. Terzis, S. P. Perlepes, et al., "Copper(II) chloride/1-methylbenzotriazole chemistry: Influence of various synthetic parameters on the product identity, structural and magnetic characterization, and quantum-chemical studies", *Inorganica Chim. Acta*, vol. 358, no. 3, Feb., 2005, pp. 565-582, doi: 10.1016/j.ica.2004.09.042

[32] N. C. Anastasiadis, G. Bilis, J. C. Plakatouras, C. P. Raptopoulou, V. Psycharis, C. Bravers, et al., "Iron(III) chloride-benzotriazole adducts with trigonal bipyramidal geometry: spectroscopic, structural and catalytic studies", *Polyhedron*, vol. 64, Nov., 2013, pp. 189-202, doi: 10.1016/j.poly.2013.03.062

[33] G. Lazari, S. Grammatikopoulos, S. P. Perlepes, T. C. Stamatatos, "Combining benzotriazoles and azides in copper(II) chemistry: Synthesis, structural and spectroscopic characterization of a 1-D corrugated tape $[Cu(N_3)_2(1\text{-Mebta})]_n$ coordination polymer (1-Mebta = 1-methylbenzotriazole)", *J. Coord. Chem.*, vol. 74, no. 11, 2021, pp. 1823-1833, doi: 10.1080/00958972.2021.1934460

[34] H. Duan, S. Sengupta, J. L. Peterson, N. G. Akhmedov, X. Shi, "Triazole-Au(I) complexes: A new class of catalysts with improved thermal stability and reactivity for intermolecular alkyne hydroamination", *J. Am. Chem. Soc.*, 131, 34, Sep., 2009, pp. 12100-12102, doi: 10.1021/ja9041093

[35] M. J. Frisch, G. W. Trucks, H. B. Schlegel, G. E. Scuseria, M. A. Robb, J. R. Cheeseman, et al., (2019). *Gaussian 16*, revision C.01, Wallingford, Connecticut: Gaussian, Inc. Available: https://gaussian.com/gaussian16

[36] Dennington, R. D. II, Keith, T. A., and Millam, J. M. (2016). *GaussView 6*, Wallingford, Connecticut: Gaussian, Inc. Available: https://gaussian.com/gaussview6

[37] R. McWeeny, "Perturbation theory for Fock-Dirac density matrix", *Phys. Rev.*, vol. 126, no. 3, May, 1962, pp. 1028-1034, doi: 10.1103/PhysRev.126.1028

[38] R. Ditchfield, "Self-consistent perturbation theory of diamagnetism. I. Gauge-invariant LCAO method for NMR chemical shifts", *Mol. Phys.*, vol. 27, no. 4, 1974, pp. 789-807, doi: 10.1080/00268977400100711

[39] J. R. Cheeseman, G. W. Trucks, T. A. Keith, M. J. Frisch, "A comparison of models for calculating nuclear magnetic resonance shielding tensors", *J. Chem. Phys.*, vol. 104, Apr., 1996, pp. 5497-5509, doi: 10.1063/1.471789 [40] J. Tomasi, B. Mennucci, R. Cammi, "Quantum mechanical continuum models", *Chem. Rev.*, vol. 105, no. 8, Jul., 2005, pp. 2999-3093, doi: 10.1021/cr9904009

[41] W. M. Haynes, Ed. *CRC Handbook of Chemistry and Physics*, 97th ed. Boca Raton, Florida, USA: CRC Press, 2017

[42] G. Socrates, *Infrared and Raman Characteristic Group Frequencies: Tables and Charts*. 3rd ed. Chichester, West Sussex, UK: Wiley, 2001

[43] B. Mennucci, J. M. Martinez, "How to Model Solvation of Peptides? Insights from a Quantum-mechanical and Molecular Dynamics Study of N-Methylacetamide. 1. Geometries, Infrared, and Ultraviolet Spectra in Water", *J. Phys. Chem. B*, vol. 109, no. 19, Apr., 2005, pp. 9818-9829, doi: 10.1021/jp050034z

[44] G. Berden, E. Jalviste, W. Leo Meerts, "Rotationally resolved UV spectroscopy of the 2*H*-tautomer of benzotriazole in a molecular beam", *Chem. Phys. Lett.*, vol. 226, no. 3-4, Aug., 1994, pp. 305-309, doi: 10.1016/0009-2614(94)00741-1

[45] W. L. F. Armarego, "Ultraviolet Spectra of Heterocycles," in *Physical Methods in Heterocyclic Chemistry*, A. R. Katritzky, Ed., New York, USA: Academic Press, 1971

[46] F. Tomás, J. Catalán, P. Pérez, J. Elguero, "Influence of lone pair repulsion vs resonance energy on the relative stabilities of molecular structures: A theoretical approach to the equilibrium between 1*H*- and 2*H*-benzotriazole tautomers", *J. Org. Chem.*, vol. 59, no. 10, May, 1994, pp. 2799-2802, doi: 10.1021/jo00089a026

[47] A. C. Borin, L. Serrano-Andrés, V. Ludwig, S. Canuto, "Theoretical absorption and emission spectra of 1H- and 2H-benzotriazole", *Phys. Chem. Chem. Phys.*, vol. 5, no. 22, 2003, pp. 5001-5009, doi: 10.1039/B310702G.